arXiv:1703.04259v2 [astro-ph.IM] 3 Apr 2017

Spatial Linear Dark Field Control: Stabilizing Deep Contrast for Exoplanet Imaging Using Bright Speckles

Kelsey Miller[a,b]
Olivier Guyon[a,b,c,d]
Jared R Males[a]

[a]Steward Observatory, University of Arizona, 933 N. Cherry Ave, Tucson, AZ 85721
[b]College of Optical Sciences, University of Arizona, 1630 E. University Blvd., Tucson, AZ 85721
[c]National Astronomical Observatory of Japan, Subaru Telescope, National Institute of Natural Sciences, Hilo, HI 96720 (USA)
[d]Astrobiology Center, National Institutes of Natural Sciences, 2-21-1 Osawa, Mitaka, Tokyo, (JAPAN)

Abstract

Direct imaging of exoplanets requires establishing and maintaining a high contrast dark hole (DH) within the science image to a high degree of precision. Current approaches aimed at establishing a DH, such as electric field conjugation (EFC), have been demonstrated in the lab and have proven capable of high contrast DH generation. The same approaches have been considered for the maintenance of the DH as well. However, these methods rely on phase diversity measurements which require field modulation; this modulation interrupts the DH and consequently competes with the science acquisition. In this paper, we introduce and demonstrate spatial linear dark field control (LDFC) as an alternative technique by which the high contrast DH can be maintained without modulation, and therefore without any disruption to the science acquisition. Spatial LDFC locks the high contrast dark field (DF) after EFC using the bright field (BF) that responds linearly to wavefront variations that modify both the BF and the DH.

Keywords: exoplanet direct imaging, high contrast imaging, wavefront control

1. Introduction

In the last two decades, the existence of over 3,000 exoplanets has been confirmed,[1] and in the upcoming era of extremely large ground-based telescopes and new space-based observatories, there is the promise of discovery, even characterization, of many more exoplanets, including potentially Earth-like worlds. With such powerful capabilities on the horizon, it has become imperative to push stellar suppression technology to higher precision in order to directly image these exoplanets. Combined with coronagraphy, current speckle nulling techniques are capable of building a DH in the science image where light from an exoplanet orbiting its star can be detected. In principle, these methods are capable of delivering 10^{-10} contrast that would enable the imaging of Earth-like exoplanets.[2] For such deep contrast levels, the generation and maintenance of the DH requires high precision measurements, and the resulting high contrast is susceptible to small aberrations found even in the most stable telescope systems. These small dynamic aberrations in the beam path produce post-coronagraph stellar light leakage and result in a quasi-static speckle field in the image plane that degrades the DH contrast over time.[3]

Techniques like speckle nulling and EFC that have proven capable of generating a DH with high contrast in the lab have also been under consideration for maintenance of the DH.[4,5] However these techniques rely on phase diversity measurements of the field at the

science detector which require field modulation.[6,7] This field modulation at the science detector, induced by a deformable mirror (DM) in a pupil plane, throws stellar light back into the DH and disrupts the science measurement. This interruption, which is required to rebuild the DH every time the contrast degrades, fundamentally limits the integration time that can be spent on any given target, and makes the use of current speckle nulling methods and EFC non-ideal for continuous maintenance of the DH.

To avoid disrupting the science measurement with field modulation to rebuild the DH, the state of the field in the DH could instead be locked once the high contrast DH has been built. To lock the state of the field, the wavefront aberrations responsible for speckle formation in the image plane must be canceled. Low-order wavefront sensing (LOWFS)[8] is a proven method designed to actively sense and correct low-order wavefront aberrations using light rejected by a reflective stop placed in a pupil plane within the coronagraph .[9,10] Here we propose two similar methods inspired by LOWFS, but with access to mid- and high-spatial frequencies. These new methods are designed to stabilize the state of the DH by using light that is outside of the DH in the spectral dimension and the spatial dimension.

The first method, referred to as spectral LDFC, freezes the state of the DH within the control bandwidth by using state measurements of light outside of the control bandwidth. This method exploits the fixed wavelength relationships that exist between speckles at different wavelengths that were generated by the same aberration. To first order, this fixed relationship scales the speckle separation linearly with wavelength and the complex amplitude as the inverse of wavelength. The complex amplitude speckle field may also interfere with static chromatic coronagraph residuals due to the coronagraph's finite design bandwidth. These relationships between out-of-band and in-band light allow for the state of the DH within the control band to be monitored and maintained by measurements made of speckles located outside of the spectral control band . The DH within the control bandwidth as well as the out-of-band speckles used by spectral LDFC to maintain the in-band DH state are shown in Fig 1 .

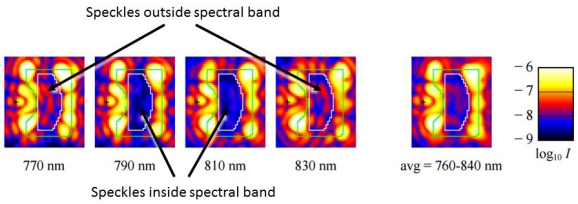

Figure 1: Spectral LDFC: The $7\lambda/D$ x $8\lambda/D$ DH from JPL's High Contrast Imaging Testbed (HCIT) created using a PIAA coronagraph. The DH is shown in four individual spectral channels: two channels within the control bandwidth and two out-of-band channels with speckles used to maintain the DH state within the control bandwidth. Also shown is the average DH over the full 10% bandwidth centered at λ = 800 nm.[11]

The second method, and topic of this paper, locks the state of the DH established by EFC using light that is spatially located outside of the DH. Spatial LDFC uses the linear signal from the strongly illuminated BF to measure the state of the field within the DH.

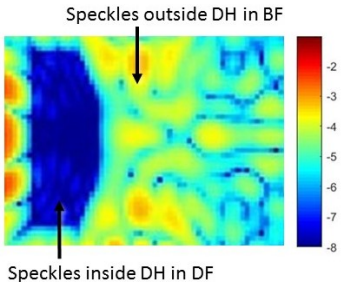

Figure 2: Spatial LDFC: $4\lambda/D$ x $10\lambda/D$ DH in simulation showing both the BF and DH within the post-EFC PSF

The purpose of this paper is to introduce spatial LDFC as a new method for DH stabilization that does not interrupt the science measurement and will consequently allow for longer, uninterrupted observing at high contrast. The concept behind spatial LDFC is laid out in section 2, and demonstrations of LDFC's abilities in simulation are shown in section 3. Further discussion of current and proposed work is laid-out in section 4 .

2. Concept

LDFC is an efficient alternative to EFC for continuous maintenance of the high contrast stellar suppression in the DH. Beginning with the DH generated by EFC, spatial LDFC provides updated information on the state of the DH by relying on intensity changes in the BF induced by changes in the wavefront. This scheme allows for constant maintenance of the contrast floor in the DH without needing to modulate the field and interrupt the science measurement to update the field estimate as is required when using EFC in closed loop to maintain the DH.

2.1. Theory

Spatial LDFC relies on the linear response of the BF to wavefront perturbations that affect both the BF and the DF; this linearity allows for a closed-loop control algorithm directly relating wavefront perturbations to changes in BF intensity. To derive the source of this linear response, we begin with the relationship between an incident wavefront and the resulting image. The complex amplitude of the incident wavefront $E_{wavefront}$ is linearly related to the complex amplitude at the image plane E_{image}:

$$E_{wavefront} \xleftrightarrow{\text{linear}} E_{image} \tag{1}$$

The same linear relationship is true with respect to E_{DM}, the multiplicative complex amplitude introduced by the DM, and the complex amplitude at the image plane.

$$E_{DM} \xleftrightarrow{\text{linear}} E_{image} \tag{2}$$

When the changes in optical path length (OPL) induced by the DM are very small such that OPL $\ll 1$, the resulting field E_t at a given time t in the image plane can be written as the sum of the initial field E_0 and the small changes in complex amplitude induced by the DM.

$$E_t \approx E_0 + E_{DM} \tag{3}$$

The resulting intensity in the image plane at time t is then given by:

$$I_t = |E_t|^2 \tag{4}$$

The total image plane intensity can be written as a sum of three terms: the intensity contribution from the initial field: $|E_0|^2$, the resulting intensity due to phase perturbations induced by the DM: $|E_{DM}|^2$, and the inner product of the initial field and the DM contribution to the complex amplitude:

$$I_t \approx |E_0|^2 + |E_{DM}|^2 + 2\langle E_0, E_{DM}\rangle \tag{5}$$

In the DF, the contribution of the initial field to the total intensity is very small, and the total intensity is dominated by the contribution of the DM such that $|E_{DM}|^2 \gg |E_0|^2$, thereby leading to a quadratic dependence of the DF on the DM input.

However, in the BF the contribution of the initial field to the total intensity dominates the contribution of the DM:

$$|E_0|^2 \gg |E_{DM}|^2 \tag{6}$$

The intensity of the BF at the image plane at time t can therefore be written as a linear dependence on the complex amplitude contribution of the DM:

$$I_t \approx 2\langle E_0, E_{DM}\rangle + |E_0|^2 \tag{7}$$

This linear response of the BF to field perturbations controlled by the DM and the quadratic response of the DF to the same DM perturbation can be seen in Fig 3 .

To demonstrate the BF and DF behavior in response to the DM field contribution E_{DM}, EFC was used to establish a DH (the DF) within a stellar PSF (the BF) in simulation. A model of a MEMs DM was then used to perturb the input wavefront by inducing a positive and negative delay in the optical path with a single actuator. This was done for a range of actuator amplitudes from -0.1 to +0.1 μm.[12] The resulting intensity response of pixels located in the DF (shown to the left in Fig 3) is governed by Eq 5 with the expected quadratic dependence on the field perturbation. The intensity response of the BF (shown to the right in Fig 3) reveals the predicted linear dependence on the DM-induced field perturbation given by Eq 7 .

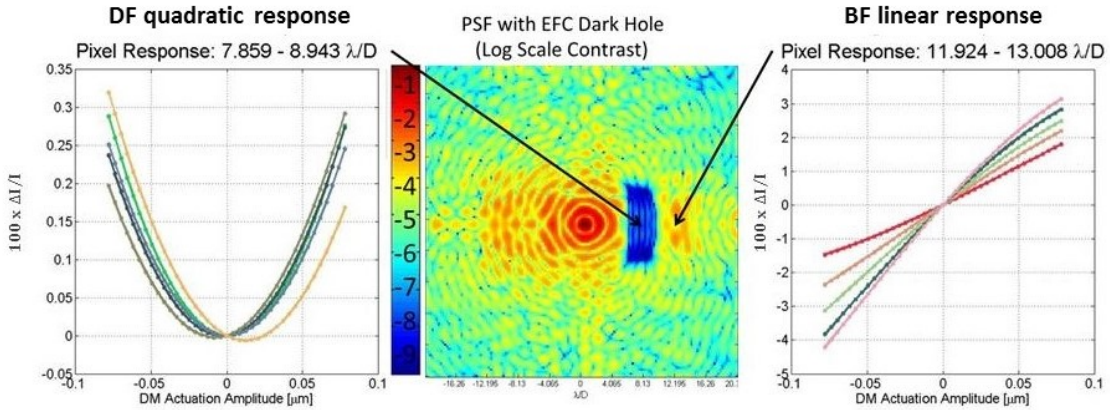

Figure 3: The response of the BF and DF to the same range of DM 'poke' amplitudes from -0.1μm to +0.1μm on a single DM actuator. Demonstrates the expected quadratic response of the DF (seen left) and the linear response of the BF (seen right) to the same range of DM poke amplitudes. Each curve in the DF image is the response of a single pixel in the DF between 8λ/D and 9λ/D, and each curve in the BF image is the response of a single pixel in the BF between 12λ/D and 13λ/D.

The linear response of the BF then allows for the construction of a linear servo driven solely by changes in the BF intensity. Unlike EFC and speckle nulling which require modulation and provide an absolute field measurement, LDFC requires no modulation and uses relative measurements of BF intensity variation in the science image. These intensity variations are used to track and cancel changes in the wavefront that modify both the BF and DF, thereby stabilizing the DF without any disruptions to the science measurement.

2.2. Calibration

Given the linear relationship between wavefront and BF intensity, using LDFC instead of EFC to stabilize the DH contrast is faster and more robust than using EFC. EFC requires multiple images to estimate the field, while each iteration of LDFC requires only one image at the science detector to determine how the field has changed with respect to the initial EFC-derived state. Since this image does not require field probing which breaks the science measurement, the LDFC servo operates with a 100% duty cycle. Furthermore, LDFC does not rely on complex field estimates which require a model-based complex phase response matrix that is difficult to measure and verify; instead, LDFC relies only on a DM $\rightarrow$ image calibration that links the shape of the DM to changes in intensity in the science image.[13]

The calibration between the image and the DM shape is obtained by building a response matrix $\mathcal{M}$ that relates the position of each individual DM actuator to the intensity variation its motion induces at the science detector. Each column of $\mathcal{M}$ records the intensity change in the science image resulting from the actuation or 'poking' of one of the k actuators on the DM that lie within the illuminated system pupil. To begin building $\mathcal{M}$, the ideal reference image I_{ref} with dimensions [n_{pix} x n_{pix}] is recorded after the DH has been established using EFC. To fill each of the k columns in $\mathcal{M}$, a single actuator is poked, the resulting perturbed image I_k is measured, and the unperturbed reference image I_{ref} is subtracted off to yield the change in intensity.

$$\mathcal{M}[:, k] = I_k - I_{ref} \tag{8}$$

This is done for all k actuators. The resulting response matrix $\mathcal{M}$ then has the dimensions [n_{pix}^2 x k].

The matrix $\mathcal{M}$ records the intensity change of both the BF and DF pixels with respect to each actuator poke. However, LDFC uses only the BF pixels which are "sufficiently bright" such that their response to wavefront perturbations is linear. The qualification "sufficiently bright" varies depending on multiple parameters including background flux, flux per speckle, detector efficiency, and SNR. Based

on these requirements, a threshold is set and applied to the initial EFC image I_{ref} which selects only the n pixels with intensities greater than or equal to the set threshold. The result is an image $I_{ref,n}$ which records the initial EFC-state of only the BF pixels. An example of this BF reference image can be seen in Fig 4 for a contrast threshold of $10^{-3.8}$.

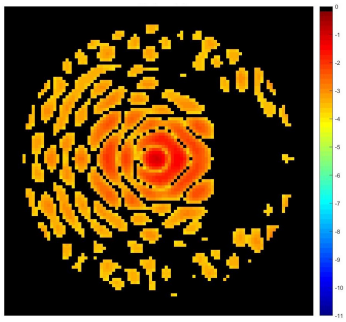

Figure 4: Image of $I_{ref,n}$ with a contrast threshold set to $10^{-3.8}$. The control area is also set to be within the control radius of the active area on the DM.

The BF response matrix M is then created by selecting the same n BF pixels from the full response matrix such that $M = \mathcal{M}_n$. The same n pixels are also selected in all future images I_t taken at a given time t .

2.3. Closed-loop implementation

To implement LDFC in closed-loop, an image I_t is taken at time t and only the n BF pixels that pass the set threshold are recorded in the BF image $I_{t,n}$. The BF reference image $I_{ref,n}$ is then subtracted from the new BF image to track the changes that have occurred in the BF with respect to the initial EFC BF reference:

$$\Delta I_{t,n} = I_{t,n} - I_{ref,n} \tag{9}$$

This BF intensity change $\Delta\, I_{t,n}$ is then fit to the pseudo-inverse of the BF response matrix M to calculate the DM shape that will return the field to its initial EFC reference state. The DM shape is represented by a vector of individual actuator amplitudes u_t:

$$u_t = -(M^T M)^{-1} M^T\, \Delta I_{t,n} \tag{10}$$

This process of taking an image, calculating the intensity change of the BF from its initial EFC reference state, and updating the DM accordingly is looped continuously to actively lock the science image field in its initial EFC state.

3. Simulation Results

To demonstrate spatial LDFC's ability to maintain the high contrast DH, a model of the testbed at the University of Arizona[1412] was built in simulation which includes a Lyot coronagraph that removes approximately two magnitudes of stellar light from the final image. For the system's deformable mirror, a model of a Boston Micromachines 1K DM was built using 1024 actuators sharing a common gaussian influence function. The system entrance pupil was set to be a 7mm diameter circular, centrally-obscured mask with spiders which lent a resulting PSF sampling in the science image of $0.27\lambda/D$ per pixel at a science wavelength of 550 nm.

With this system built in simulation, a standard implementation of EFC[7] was then used to suppress the stellar light in a given region next to the PSF core to an average contrast floor of 10^{-8} (seen in Fig 5). This resulting DH was then the ideal reference state for LDFC to maintain, and the intensity image I_{ref} was saved as the reference image to be used in the LDFC servo to return the DH to its EFC-derived state.

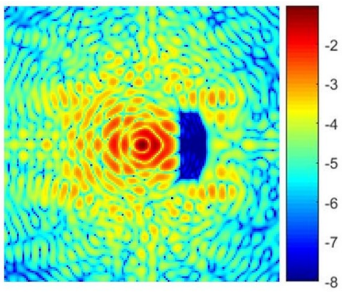

Figure 5: Image of $\log_{10}(I_{ref})$ with average DH contrast = 10^{-8} at t = 0 taken immediately after implementing EFC

Once the DH was built, a spatial sine wave phase perturbation was introduced into the pupil plane, forming a speckle in the DH as well as in the BF on the opposite side of the PSF.

The LDFC algorithm was then implemented as described in section 2.3 to sense the resulting change in the BF and counteract it using the model DM to apply the conjugate phase.

Presented below are two specific demonstrations of spatial LDFC: one case with an injected speckle amplitude small enough to fall within the algorithm's linear regime, and a second case with a higher speckle amplitude which falls outside the algorithm's linear regime. For both demonstrations, the same pupil, and consequently the same number of illuminated active actuators on the DM, were used to build the DH and implement the LDFC closed loop test. Using the same science wavelength as well as the same entrance pupil diameter also preserved the sampling at the science detector. The threshold for defining the BF and the subsequent number of BF pixels used in the LDFC servo were also kept constant for both demonstrations. All of these parameters can be found in Table 1.

Science wavelength	550 nm
Pupil diameter	7 mm
Sampling at detector	0.27 λ/D per pixel
# DM actuators used	398
# Bright field pixels used	5002
Bright field contrast threshold	$10^{-4.8}$

Table 1: Simulated system parameters used in both of the following LDFC demonstrations

3.1. Linear regime

Using the system described above, a spatial sine wave phase perturbation was introduced into the pupil plane, producing a speckle with a maximum magnitude of $10^{-5.1}$. This amplitude was low enough to remain within the servo's linear regime, and the algorithm converged to 0.98x the initial $\log_{10}$ EFC contrast after only one iteration. The results of this demonstration are given in Table 2 .

EFC DH contrast	$10^{-8.0}$
Speckle magnitude	$10^{-5.1}$
Avg DH contrast with speckle	$10^{-6.9}$
LDFC DH contrast	$10^{-7.8}$
ΔContrast	$10^{-0.9}$
# Iterations to converge	1

Table 2: Linear regime results: Initial EFC DH average contrast, the magnitude of the injected speckle, the average contrast of the DH with the speckle, the average contrast of the DH after LDFC, the total change in contrast for one LDFC loop, and the number of iterations to converge to 0.98x the $\log_{10}$ EFC contrast floor

Visualization of the linear-regime results and a plot of the convergence of the DH contrast to the initial EFC contrast floor are given in Fig(s) 6 - 8 .

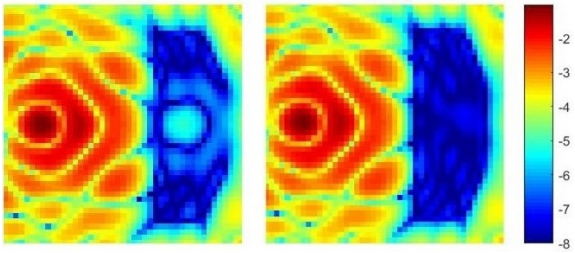

Figure 6: DH before and after LDFC
(Left) Injection of a $10^{-5.1}$ magnitude speckle yielding a degraded DH average contrast of $10^{-6.9}$.
(Right) Final LDFC-corrected DH with an average contrast of $10^{-7.8}$ achieved after 1 iteration.

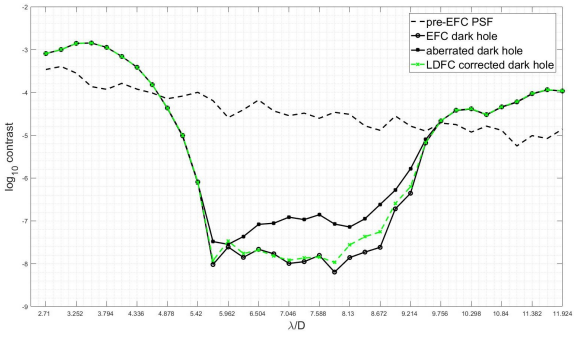

Figure 7: Average contrast curves across the full DH: pre-EFC PSF, DH post-EFC, DH post-EFC with injected speckle, corrected DH post-LDFC (green)

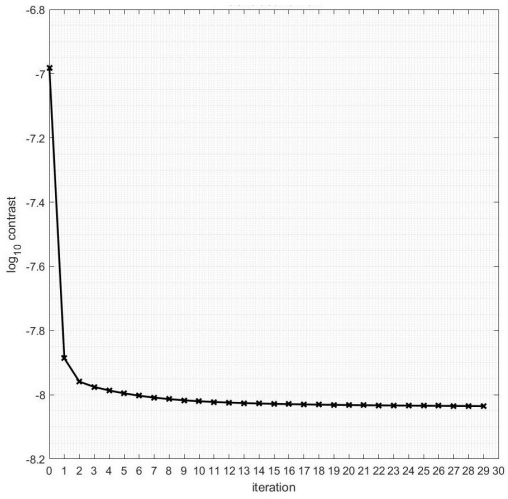

Figure 8: LDFC contrast vs iteration: DH contrast over 30 LDFC iterations showing convergence to 0.98x the initial $\log_{10}$ EFC contrast after 1 iteration and the following EFC-level plateau at 10^{-8}

3.2. Non-linear regime

For the second demonstration, a spatial sine wave phase perturbation with twice the complex amplitude of the first demonstration was introduced into the pupil plane, producing a speckle with a maximum magnitude of $10^{-4.5}$. This amplitude fell outside the servo's linear regime, and the algorithm converged to 0.98x the initial $\log_{10}$ EFC contrast after two iterations. The results of this demonstration are given in Table 3 .

EFC DH contrast	$10^{-8.0}$
Speckle magnitude	$10^{-4.5}$
Avg DH contrast with speckle	$10^{-6.5}$
LDFC DH contrast	$10^{-7.9}$
ΔContrast	$10^{-1.4}$
# Iterations to converge	2

Table 3: Non-linear regime results: Initial EFC DH average contrast, the magnitude of the injected speckle, the average contrast of the DH with the speckle, the average contrast of the DH after LDFC, the total change in contrast for one full LDFC loop (in this case, 2 iterations), and the number of iterations to converge to 0.98x the $\log_{10}$ EFC contrast floor

Visualization of the nonlinear-regime results and a plot of the convergence of the DH contrast to the initial EFC contrast floor are given in Fig(s) 9 - 11 .

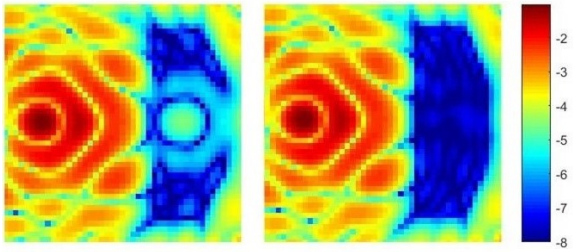

Figure 9: DH before and after LDFC
(Left) Injection of a $10^{-4.5}$ magnitude speckle yielding a degraded DH average contrast of $10^{-6.5}$.
(Right) Final LDFC-corrected DH with an average contrast of $10^{-7.9}$ achieved after 2 iterations.

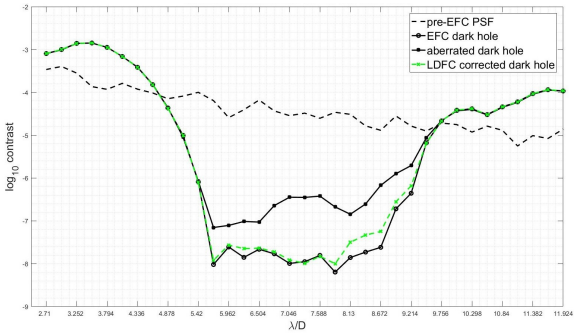

Figure 10: Average contrast curves across the full DH: pre-EFC PSF, DH post-EFC, DH post-EFC with injected speckle, corrected DH post-LDFC (green)

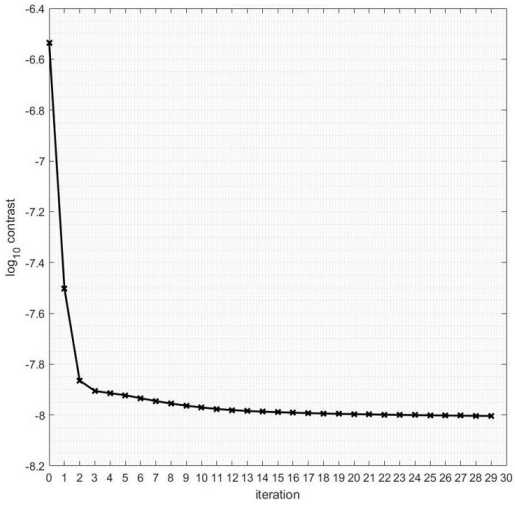

Figure 11: LDFC contrast vs iteration: DH contrast over 30 LDFC iterations showing convergence to 0.98x the initial $\log_{10}$ EFC contrast after 2 iterations and the following EFC-level plateau at 10^{-8}

4. Discussion

In summary, spatial LDFC acts as an extension of EFC by operating as a servo that can maintain high contrast in the DH during science exposures. Using changes in the BF to provide updates on the state of the field within the DH, spatial LDFC is able to lock the state of the DH after it is established by EFC without relying on field modulation which interrupts the science acquisition and fundamentally limits the exposure time. This ability makes spatial LDFC a more efficient method than EFC for maintaining the deep contrast within the DH.

We have demonstrated here that spatial LDFC is capable of locking the DH contrast at its ideal EFC state using only the BF response to a perturbation in the optical path, even when the amplitude of that perturbation is high enough to fall outside of the linear regime of this technique. It should be noted that this paper has specifically explored aberrations introduced and corrected by the same DM, and in reality there will be aberrations that do not correspond exactly to DM authority. Exploration of spatial LDFC's response to this phenomenon and further algorithm development are left for future work. Another key issue to be explored is the mapping of spatial LDFC's null space, (i.e. wavefront errors that affect the DF without changing the BF).

5. Acknowledgments

The technique presented here was first conceived by Dr. Olivier Guyon, and this work was funded by the NASA Exoplanet Exploration program Segmented Coronagraph Design and Analysis study effort. The author would like to acknowledge Dr. Sandrine Thomas for her assistance in implementing EFC in for this work. For their continued support, the author also acknowledges fellow members of Dr. Guyon's and Dr. Male's research group: Justin Knight, Jennifer Lumbres, Alexander Rodack, and Lauren Schatz.

References

[1] "NASA Exoplanet Science Institute: NASA Exoplanet Archive." `http://exoplanetarchive.ipac.caltech.edu/cgi-bin/TblView/nph-tblView?app=ExoTbls&config=planets`. Accessed: 03/2017.

[2] J. T. Trauger and W. A. Traub, "A laboratory demonstration of the capability to image an earth-like extrasolar planet," *Nature* **446**, pp. 771–773, Apr 2007.

[3] W. Traub and B. Oppenheimer, "Direct imaging of exoplanets," 2010. Exoplanets (Tucson: Univ. Arizona Press).

[4] E. Cady, C. Baranec, C. Beichman, D. Brenner, R. Burruss, J. Crepp, R. Dekany, D. Hale, L. Hillenbrand, S. Hinkley, E. R. Ligon, T. Lockhart, B. Oppenheimer, I. Parry, L. Pueyo, E. Rice, L. C. Roberts, J. Roberts, M. Shao, A. Sivaramakrishnan, R. Soummer, H. Tang, T. Truong, G. Vasisht, F. Vescelus, J. K. Wallace, C. Zhai, and N. Zimmerman, "Electric field conjugation with the project 1640 coronagraph," 2013.

[5] J.-B. Ruffio, "Non common path aberrations correction," Master's thesis, ESO Adaptive Optics Department, 2014.

[6] A. Give'on, B. Kern, S. Shaklan, D. C. Moody, and L. Pueyo, "Broadband wavefront correction algorithm for high-contrast imaging systems," 2007.

[7] T. D. Groff, A. J. Eldorado Riggs, B. Kern, and N. Jeremy Kasdin, "Methods and limitations of focal plane sensing, estimation, and control in high-contrast imaging," *Journal of Astronomical Telescopes, Instruments, and Systems* **2**(1), p. 011009, 2015.

[8] O. Guyon, T. Matsuo, and R. Angel, "Coronagraphic low-order wave-front sensor: Principle and application to a phase-induced amplitude coronagraph," *The Astrophysical Journal* **693**(1), p. 75, 2009.

[9] G. Singh, J. Lozi, O. Guyon, P. Baudoz, N. Jovanovic, F. Martinache, T. Kudo, E. Serabyn, and J. Kuhn, "On-sky demonstration of low-order wavefront sensing and control with focal plane phase mask coronagraphs," *Publications of the Astronomical Society of the Pacific* **127**(955), p. 857, 2015.

[10] F. SHI, "Low Order Wavefront Sensing and Control for WFIRST-AFTA Coronagraph," in *American Astronomical Society Meeting Abstracts*, *American Astronomical Society Meeting Abstracts* **227**, p. 430.04, Jan. 2016.

[11] O. Guyon, B. Kern, A. Kuhnert, and A. Niessner, "Phase-induced amplitude apodization (piaa) technology development, milestone 3: 10% bandpass contrast demonstration," May 2014. Technology Development for Exoplanet Missions Technology Milestone Report.

[12] K. Miller and O. Guyon, "Linear dark field control: simulation for implementation and testing on the ua wavefront control testbed," 2016.

[13] O. Guyon, J. Codona, K. Miller, J. Knight, and A. Rodack, "Wavefront sensing, control, and psf calibration," February 2015. NASA-JPL LOWFSC Conference.

[14] K. Miller, O. Guyon, J. Codona, J. Knight, and A. Rodack, "Ua wavefront control lab: design overview and implementation of new wavefront sensing techniques," 2015.